FIV2024
IGUAÇU FALLS, BRAZIL
2-5 JULY 2024

FIV2024: FSI² & FIV + N
10th International Symposium on Fluid-Structure Interactions,
Flow-Sound Interactions, Flow-Induced Vibration & Noise

FIV2024-0101
SUBMERGED CANTILEVERED FLEXIBLE PIPE DISCHARGING FLOW IN POST-CRITICAL DYNAMIC REGIME: AN EXPERIMENTAL-NUMERICAL ASSESSMENT

Wagner Antonio Defensor Filho
Renato Maia Matarazzo Orsino
Guilherme Jorge Vernizzi
Guilherme Rosa Franzini
Celso Pupo Pesce
Escola Politécnica da Universidade de São Paulo – Offshore Mechanics Laboratory. Av. Prof. Lúcio Martins Rodrigues, Travessa quatro, 434, Campus da USP – Butantã, São Paulo – SP, 05508-020
wadfilho@usp.br, reorsino@usp.br, guilherme.jorge.lopes@usp.br, gfranzini@usp.br, ceppesce@usp.br

Abstract. *This work presents experimental results and comparison with a numerical model for the problem of a flexible pipe conveying fluid in post-critical regime while immersed in still water. The measurements were made with an optical tracking system in order to avoid interference with the fluid and the model, while providing a direct measure of the displacements of various cross-sections. The results show that, even though the numerical model is able to correctly predict the existence of a critical discharging velocity above which the vertical equilibrium configuration becomes unstable and the system exhibits a steady state non-linear oscillatory response, the actual dynamics of the problem is richer than what was expected in the numerical modelling. The experimental response includes the appearance of a dual resonance and motion patterns different from the reported behavior for a flexible pipe conveying fluid in air, that go beyond the effect of a classical Morison drag term. The results allow to conclude that there are fluid-structure interaction phenomena occurring that have not yet been explored for this particular problem and require further investigation through appropriate numerical modeling.*

Keywords: *Flexible Pipes, Internal Flow, Discharging, Instability, Reduced-Order Model*

1. INTRODUCTION

Since the advent of offshore risers in the Oil industry in the 50's and 60's, especially the introduction of flexible risers in the 70's, the industry demanded a better understanding of the dynamics of these pipes, particularly of the internal flow effects on the well-established understanding of vortex-induced vibration phenomena. The use of heat exchangers in industry has also greatly contributed to further investigations into the dynamics of pipes subjected to the concomitant actions of internal and axial external flows. As required, most of these investigations focused on configurations pertinent to offshore risers and heat exchangers, more specifically in pinned-pinned and camped-clamped systems.

Rich discussions and overviews can be found in Païdoussis (1998) and Païdoussis (2022), respectively, regarding different topics on the dynamics of slender structures subjected to internal and external flows, either separately or simultaneously, as well as a conductor thread over the numerous studies on the theme.

The dynamics of cantilevered flexible pipes discharging fluid have primarily been of academic interest since its industrial application was practically non-existent. This particular configuration is widely known as Benjamin's problem, in recognition for its establishment of the basis of understanding concerning the dynamics of this type of system (Benjamin, 1961). Benjamin identified through a stability analysis that, as the discharging flow exceeds a specific velocity, the vertical equilibrium configuration becomes unstable and the system exhibits self-excited oscillations. Such a velocity value is referred as internal flow *critical velocity*.

In recent years, seawater intake risers (SWIRs) have been increasingly used in the offshore industry as a means of reducing its carbon footprint. SWIRs are long cantilevered flexible pipes fixed to a vessel's hull, used to aspirate cold seawater from great depths. The aspirated water is used in the vessel's cooling system thus increasing its efficiency due to the greater temperature difference compared to a recirculating cooling system. This new type of industrial use opens space to new studies which may also consider cantilevered flexible pipes discharging fluid.

Mathematically modelling a cantilevered flexible pipe discharging fluid in the post-critical regime is a challenging task due to the high complexity and nonlinear dynamic behavior. This task is further complicated when the pipe is submerged, as the interaction with the external medium becomes relevant and adds complexity to the overall phenomena. Therefore, robust consistency between the internal and external flows modelling is crucial.

Aiming to address this issue, this work presents an experimental-numerical comparison of a submerged cantilevered flexible pipe discharging water in the post-critical regime. Benchmark results were obtained from a unique experimental campaign carried out at the towing tank facility of the Instituto de Pesquisas Tecnológicas do Estado de São Paulo (IPT), using an optical tracking system to capture the experimental model dynamics. To the best of the authors' knowledge, this methodology has no precedent in the related technical literature and the results represent a new paradigm.

Aiming at reproducing the dynamics exhibited in the experiments, a numerical model of a cantilevered flexible pipe, initially developed to assist in designing the experimental model and selecting the scenarios to be tested, is now simulated replicating the test conditions. This numerical code is under continuous development at the Offshore Mechanics Laboratory and is henceforward referred as the *in house-model*.

2. EXPERIMENTAL METHODOLOGY

Figure 1(a) shows the set of the three experimental models used in the test campaign, mounted in the testing position of the towing tank. The experimental models were developed based on a fundamental rather than scaled SWIR concept. As a fundamental concept, it was established that the experimental models (i) would consist of a flexible hose with a rigid ballast attached at its inferior free end, and (ii) both the hose and the ballast would present the same internal and external diameters in order to avoid undesired hydrodynamic interferences. The selected pipe was a rubber hose with an internal fiber reinforcement layer. For the ballast, brass was chosen due to its high density and good machinability. The present work focuses on the longest experimental model, presented in the center of the aforementioned figure, named as BH-3, referencing the ballasted-hose concept.

A dynamic characterization of the hose material provided its axial and bending stiffnesses. The brass nominal mechanical parameters were adopted under the hypothesis that any value variation would not interfere in the model dimensioning since the hose presents a much higher flexibility. Both the hose and the ballast had their linear density measured. Table 1 and Table 2 present, respectively, the main parameters, and the natural frequencies measured in still water through vibration decay tests.

Based on the measured parameters of the experimental model, the mathematical model was used to identify the nominal value for the internal flow critical velocity, through the Argand diagram depicted in Figure 1(b). The Argand diagram shows the values of the experimental model's natural periods as function of the discharging flow velocity, considering the model submerged in its trivial equilibrium vertical configuration, and in the absence of external flow. The natural modes are ordered from top to bottom. Blue colors indicate negative real parts for the corresponding eigenvalues (stability) and red colors indicate positive real parts (instability). The first mode to shift from stable to unstable regime is the third natural mode, at the discharging flow velocity of $V = 6.35$ m/s.

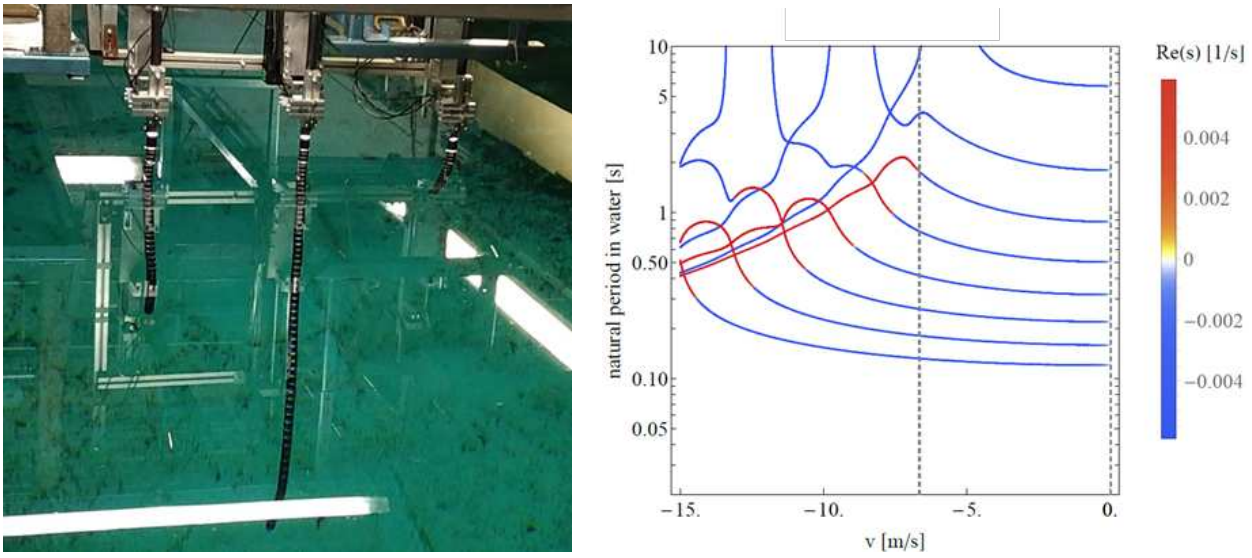

(a) (b)

Figure 1. (a) Experimental models in test position. Model BH-3 at the center. (b) *Root-loci* diagram for the model BH-3, using as-built parameters (in the scope of the experimental campaign, a negative sign convention was adopted for discharging flow velocities).

A wireless optical tracking system with underwater cameras was used for recording the model's dynamics. The optical system tracked the displacements of several reflective tapes attached along the model length (as shown in Figure 1(a)), interpreting each one as a 3D Cartesian coordinate frame in space. The discharging flow velocity was gradually increased to $V = 6.526$ m/s, a value slightly higher than the nominal critical velocity. The analysis focused on the stationary

post-critical dynamic regime, not considering the initial and final transients.

Table 1. Experimental model BH-3 parameters.

	Parameter	Model
Hose – Nitrile rubber	Linear density [kg/m]	0.56
	Axial stiffness (EA) [N]	12.5 10^3
	Bending stiffness (EI) [Nm^2]	1.23
	Length [m]	2.857
	Mass [kg]	1.60
Ballast - Brass	Linear density [kg/m]	4.15
	Axial stiffness (EA) [N]	49.9 10^6
	Bending stiffness (EI) [Nm^2]	4.91 10^3
	Length [m]	0.173
	Mass [kg]	0.72
Complete model	External diameter [mm]	33
	Internal diameter [mm]	22
	Length ratio (ballast to hose) [%]	6.06
	Total length [m]	3.030
	Slenderness (length to ext. diameter ratio)	91.82
	Mass [kg]	2.32
	Mass of water inside the pipe [kg]	1.15
	Mass of water displaced by the pipe [kg]	2.59
	Discharging critical velocity [m/s]	6.35

Table 2. Experimental model BH-3 natural frequencies in water (at $V = 0$).

Direction	Natural frequency [Hz]		
	Mode 1	Mode 2	Mode 3
x	0.18	0.56	1.17
y	0.17	0.56	1.15

3. THE IN-HOUSE MODEL

The *in-house model* corresponds to a 3D reduced-order mathematical model (ROM) derived through the application of the generalized form of Hamilton's principle for non-material volumes proposed by Casetta and Pesce (2013), consistently accounting for the dynamic effects of the flow discharging at the free end of the pipe. The derivation follows the same hypotheses and formulation of the model originally introduced in Orsino *et al.* (2018), apart from the fact that, in the present case the pipe includes not only the hose segment, modelled as an inextensible, homogeneous and linear elastic beam (which can perform large displacements with small strains), but also a ballast segment, modelled as a rigid body. Another difference of the model adopted in the present paper when compared to the one in Orsino *et al.* (2018) is that, since there is no towing in the experiments considered herein, the fluid structure interactions with the external flow take into account only added mass and pure drag effects (according do Morison's formula), i.e., no VIV phenomenological model is assumed for the present case.

Choosing the length $L = L_\mathrm{h} + L_\mathrm{b}$ of the pipe (hose + ballast), the mass m_d of water displaced due to the presence of the pipe and $t_\mathrm{ref} = \sqrt{m_\mathrm{d} L_\mathrm{h}^3 / EI}$ as the reference scales for length, mass and time, respectively, the whole formulation can be obtained in *non-dimensional* form. Using notation conventions similar to the ones adopted in Orsino *et al.* (2018) the non-dimensional Lagrangian and non-dimensional virtual work of non-conservative forces (including the effects of flux of momentum due to the ejection of fluid) are given respectively by:

$$\mathcal{L} = \frac{1}{2}\int_0^1 \Bigg[\underbrace{\mu_\mathrm{p}\left|\dot{\vec{\mathrm{r}}}\right|^2}_{\text{pipe inertia}} + \underbrace{\mu_\mathrm{i}\left|\dot{\vec{\mathrm{r}}} + v\vec{\mathrm{r}}'\right|^2}_{\text{internal flow inertia}} + \underbrace{\dot{\vec{\mathrm{r}}}\cdot\mathrm{M}_\mathrm{a}\cdot\dot{\vec{\mathrm{r}}}}_{\text{added mass}} - \underbrace{2\gamma(1-\mu_\mathrm{p}-\mu_\mathrm{i})(\vec{\mathrm{r}}\cdot\hat{\mathrm{n}}_\mathrm{z})}_{\text{buoyancy and gravity}} \Bigg]\mathrm{d}s - \frac{1}{2}\int_0^{l_\mathrm{h}} \underbrace{\vec{\mathrm{r}}''\cdot\vec{\mathrm{r}}''}_{\text{flexural stiffness}}\,\mathrm{d}s \tag{1}$$

$$\delta\tilde{W} = \int_0^1 \Bigg\{ \underbrace{-\frac{2C_\mathrm{D}}{\pi d_\mathrm{e}}\left|\dot{\vec{\mathrm{r}}}\right|\dot{\vec{\mathrm{r}}}}_{\text{drag}} \underbrace{-\beta\dot{\vec{\mathrm{r}}}}_{\text{damping}} \Bigg\}\cdot\delta\vec{\mathrm{r}}\,\mathrm{d}s - \underbrace{\left[\mu_\mathrm{i} v\left(\dot{\vec{\mathrm{r}}} + v\vec{\mathrm{r}}'\right)\cdot\delta\vec{\mathrm{r}}\right]_{s=1}}_{\text{flux of momentum}} \tag{2}$$

Basically, s denotes a non-dimensional arc-lenght coordinate: $0 \leq s \leq l_\mathrm{h}$ is the hose segment and $l_\mathrm{h} < s \leq 1$ is the ballast segment; $\vec{\mathrm{r}}$ denotes the non-dimentional position vector of points along the center line of the pipe, with $\dot{\vec{\mathrm{r}}}$ denoting its non-dimensional time derivative and $\vec{\mathrm{r}}' = \partial\vec{\mathrm{r}}/\partial s$, being the corresponding local tangent unit vector. The other *non-dimensional parameters* that appear in the formulation are:

- l_h: hose length;
- μ_p: linear mass density of the pipe;
- μ_i: linear mass density of the fluid inside the pipe;
- v: relative velocity of the plug flow internal to the pipe;
- $\mathrm{M_a}$: added mass tensor;
- $\gamma = gL^2 m_\mathrm{a}/EI$: geometric to bending stiffness ratio;
- C_D: drag coefficient;
- d_e: external diameter of the pipe;
- β: linear damping coefficient of the structure (from free oscillation decay tests performed in air $\beta = 0.21$).

A Galerkin projection scheme with a set of 5 projection functions, corresponding to the first five modal shapes of a clamped-free linear Euler-Bernoulli beam, is used to discretize all the variables defined along the length of the pipe, leading to the derivation of a non-linear reduced-order model.

The ordinary differential equations (ODEs) so obtained are symbolically generated in Wolfram Mathematica© and numerically simulated in Julia Language, using the build-in implementation of the Bogacki-Shampine 3/2 Runge-Kutta method available in the package DifferentialEquations.jl. In the simulation, the internal plug flow velocity is assumed to be equal to the one measured in the experimental tests, $V = 6.526$ m/s, slightly above the nominal critical velocity $V = 6.35$ m/s, above which, according to the stability analysis performed with the linearized form of the equations of motion, the real part of at least one eigenvalue of the system becomes positive. The initial conditions are sufficient to provide a small deviation from the (unstable equilibrium) vertical configuration.

The numerical results presented in the next section focus primarily on the steady state non-linear oscillatory response of the system, which is not affected by the transient effects observed at the beginning of the time series obtained in the simulation.

4. RESULTS COMPARISON

This section addresses the comparison between the experimental and numerical results. For both cases, the set of results are analogous, consisting of displacement trajectories and amplitude spectra.

This analysis starts by the experimental model's dynamics. Figures 2(a), (b) and (c), show the orbital projections onto the xz, yz and xy (horizontal) planes, respectively, referring to eight arc-length positions, $S = z_0/L = 0.00, 0.13, 0.29, 0.45, 0.61, 0.77, 0.90$ and 1.00, with z_0 and L being the initial vertical position and the model length, respectively. Large amplitude displacements of the tip reach approximately $a_x^* = a_x/L = 0.3$ and $a_y^* = a_y/L = 0.4$ in the x and y directions, respectively. Notice in Fig. 2(c) that the projection of the displacements in the xy plane are not centered in the origin, even though there is no external flow present. This effect is caused by a residual curvature in the hose due to its manufacture process and subsequent coiled storage. Figure 2(d) depicts 3D orbits along with a black vertical line illustrating the hose configuration at a specific instant of time. This configuration was obtained with a pre-processing algorithm for reconstructing lost signals (Vernizzi *et al.*, 2023). Displacement gaps can be noticed at the tip trajectory, coming from measured frames in which the underwater cameras' volume of capture was exceeded. Well-defined eight-shape trajectories are depicted in Fig. 2(e) and (f) through snapshots of the deformed non-linear configurations. The corresponding results for the numerical model are shown in Fig. 3.

Three main differences are noticeable between the results. Firstly, the projection of the motion in the xy plane is centered in zero for the numerical model, which is expected since it is assumed to be ideally axisymmetric (not containing the residual deformations present in the experimental model). The other two aspects that differ between models, however, do not permit such a simple explanation. The amplitudes of motion obtained from the numerical model are large, but not as large as the experimental results show. Additionally, the eight-shape pattern of motion is not recovered with the numerical simulations.

Regarding the difference in amplitude, it can be observed in the instantaneous displaced configuration (Figs. 2(e) and (f)) a significant motion in the axial direction of the pipe. This direction of motion leads to the development of smaller drag forces during the motion, which may be one of the factors resulting in very large amplitudes achieved by the experimental

model, deserving further investigation. Returning to the mathematical model, it should be noticed that axial inextensibility condition is assumed for the displacement fields, which means that the numerical simulations will not reproduce the axial dynamics. This becomes then an observation for the development of future mathematical models, which is the necessity of including the axial dynamics, even if the axial stretch is expected to be small.

In order to explain the differences in the pattern of motion, consider the results in Fig. 4, showing the tip displacements with the respective amplitude spectra for both models, alongside the results in Fig. 5, which show the amplitude spectra along the entire length of the models.

For the experimental results, dominant peaks with frequencies of 0.48 Hz and 0.24 Hz are highlighted in the x and y directions, respectively. This 2:1 frequency ratio in the response of displacements that are orthogonal to each other indicates a dual resonance in the dynamics of transverse modes, resulting in figure-of-eight-shape trajectories. Notice that the experimental model presents a 2:1 ratio between the frequencies corresponding to the third and second natural modes of vibration. However, the peaks in Fig. 4(a) do not match the values of the natural frequencies neither are in harmonic relationship with them. Additionally, the results in Fig. 5(a) show that this dual relationship is maintained along the entire length of the hose.

Since the frequencies obtained from the amplitude spectra are not the natural frequencies of the model in water, neither are in harmonic relationship with such frequencies, the resulting motion in the figure-of-eight-shaped pattern is likely due to a fluid-structure interaction phenomenon, which may be triggered by the existence of the 2:1 ratio in the natural modes of the pipe, since other similar model that was experimentally tested in the post-critical discharging flow condition but did not have such a relationship in its natural modes presented only oval shapes in the trajectories (see Defensor Filho *et al.* (2023)).

The statement of the fluid-structure interaction origin for the trajectories is further reinforced by the results of the numerical model. For this case, only the drag force was considered in the phenomenology, and as the results show, the response consists only of the oscillations of the mode that becomes unstable for the internal flow velocity investigated, with a slightly higher frequency than the natural one. This frequency shift can be seen in Fig. 1(b) as well, with the increase of the imaginary part of the eigenvalue associated with the third mode at the value of critical velocity. From this is possible to conclude that the structural modelling and the drag force modelled using the Morison formula alone are not able to capture what actually happens in the experiment, suggesting the existence of un-modelled aspects of fluid-structure interaction.

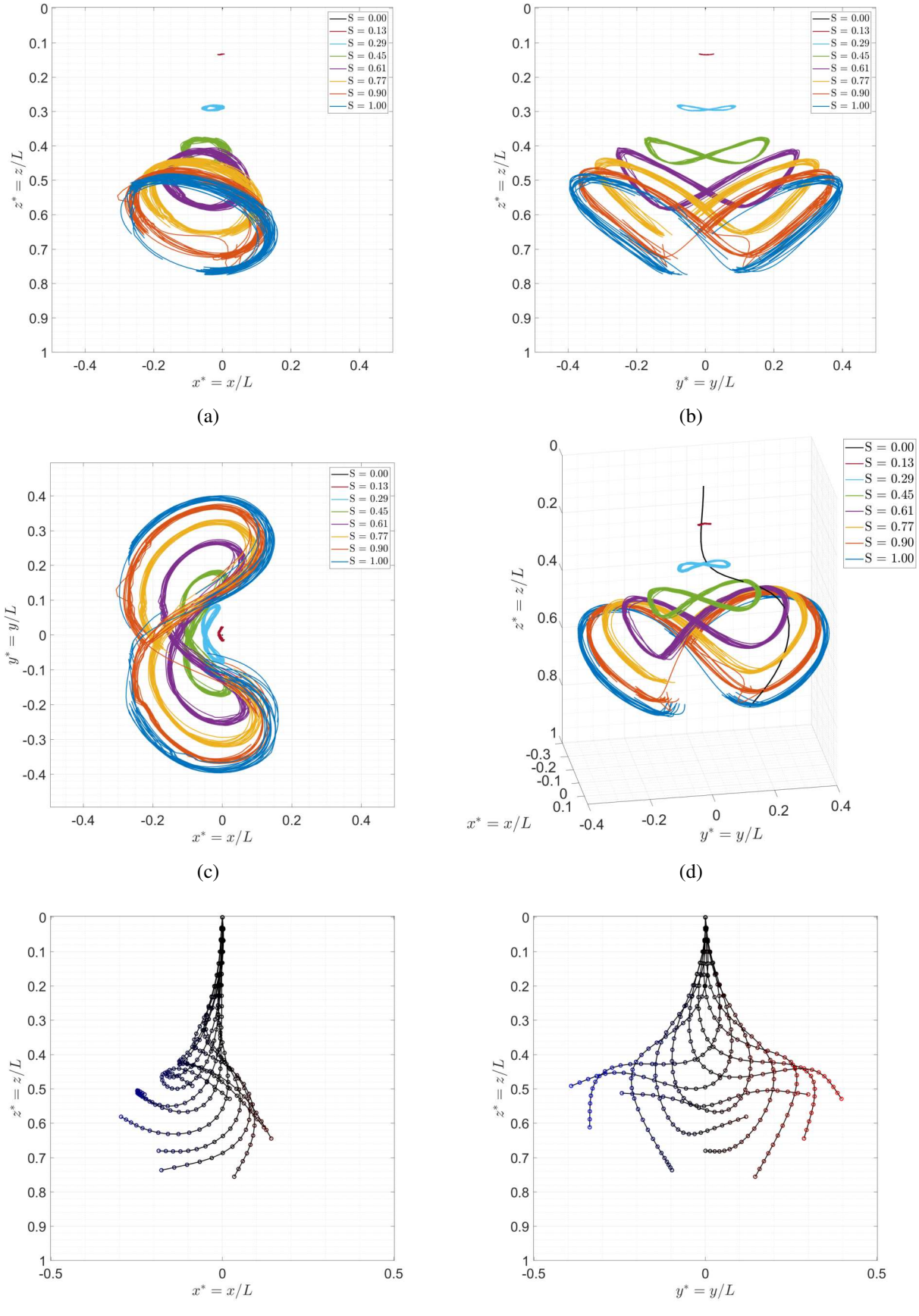

Figure 2. Experimental model. (a), (b) and (c) Orbits projections onto the xz, yz and xy (horizontal) planes, respectively. (d) Three-dimensional orbits. (e) and (f) Deformed configuration snapshots in the x and y directions, respectively, along the vertical axis. Red colors: positive coordinates; blue colors: negative coordinates. Scales 1:1.

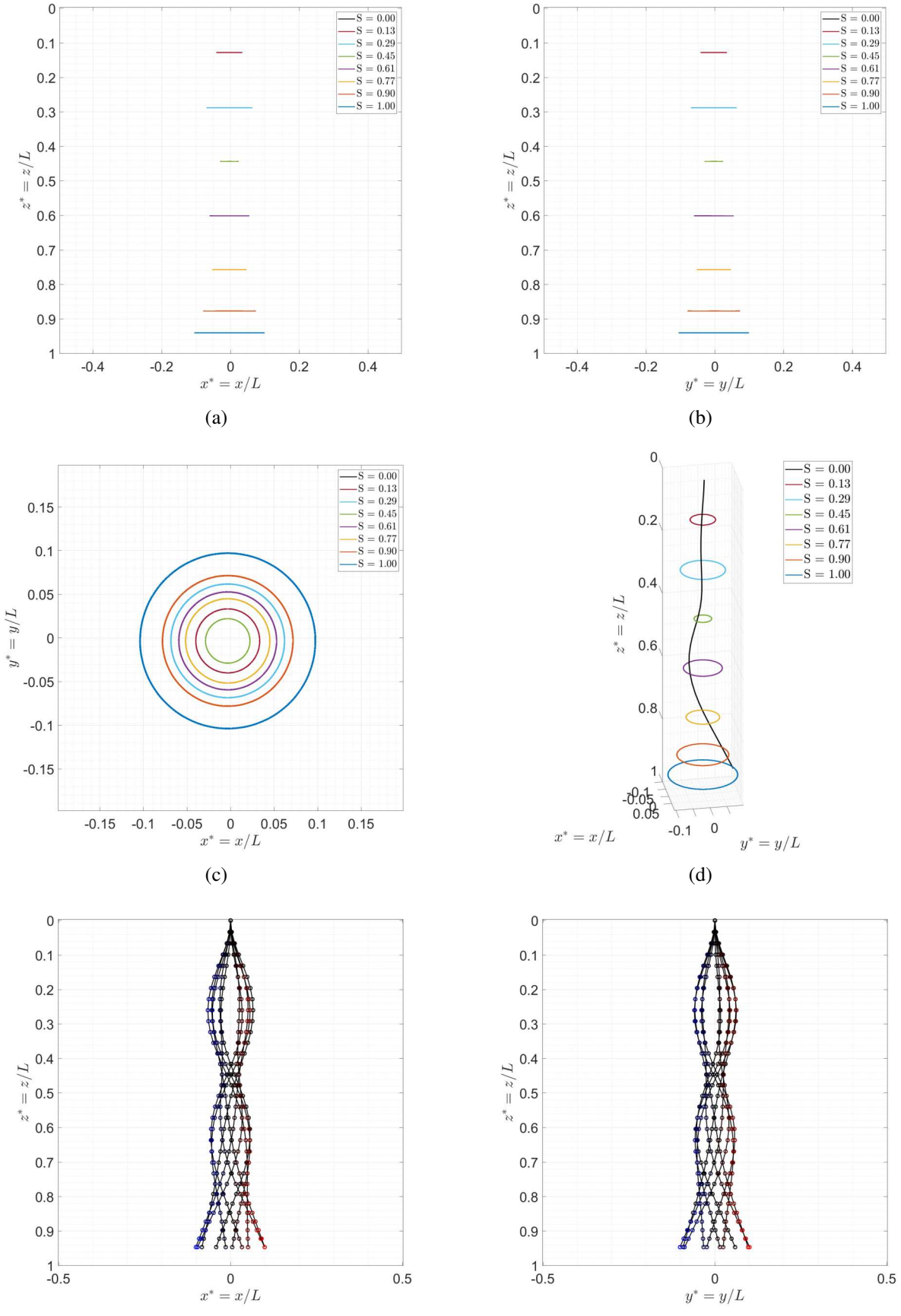

(a) (b) (c) (d) (e) (f)

Figure 3. Numerical model. (a), (b) and (c) Orbits projections onto the xz, yz and xy (horizontal) planes, respectively. (d) Three-dimensional orbits. (e) and (f) Deformed configuration snapshots in the x and y directions, respectively, along the vertical axis. Red colors: positive coordinates; blue colors: negative coordinates. Scales 1:1.

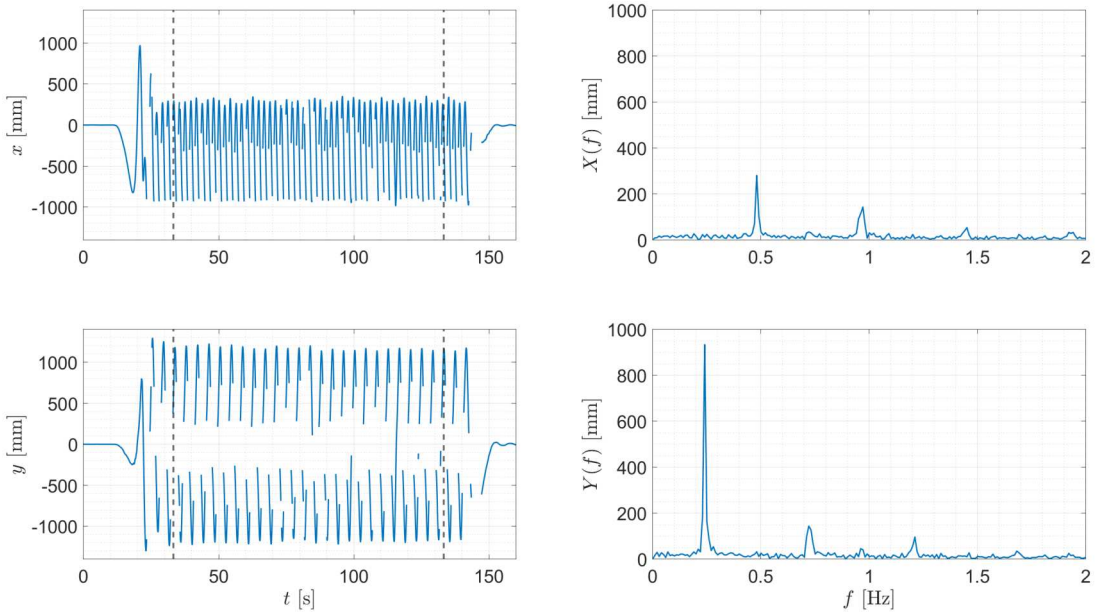

(a)

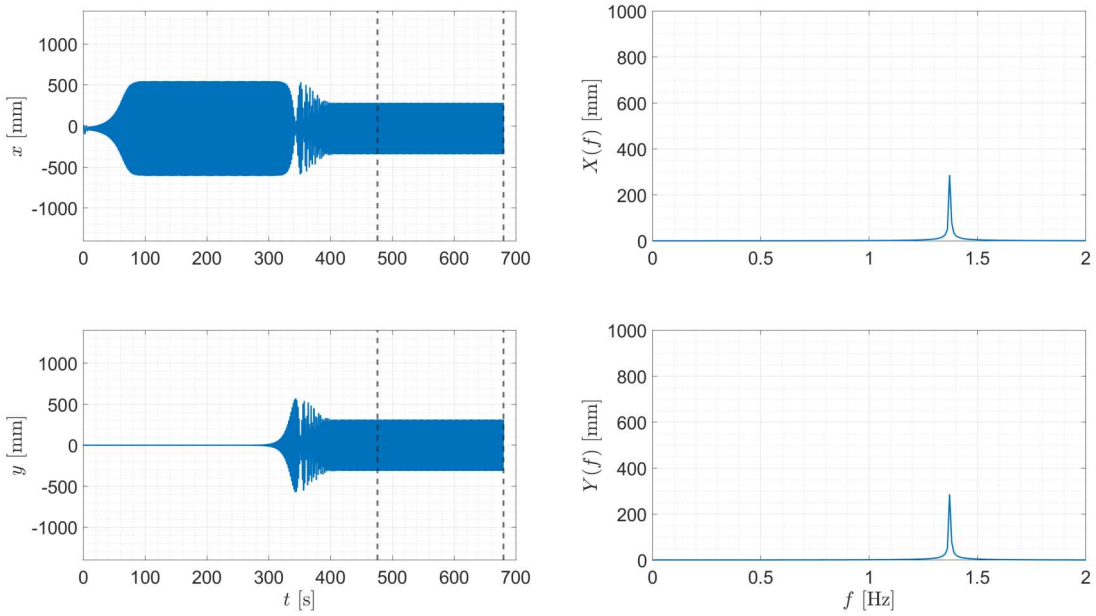

(b)

Figure 4. Tip time series and the respective spectrum in the x and y directions. Vertical dashed lines indicate the selected part of the signal. (a) Experimental model. (b) Numerical model.

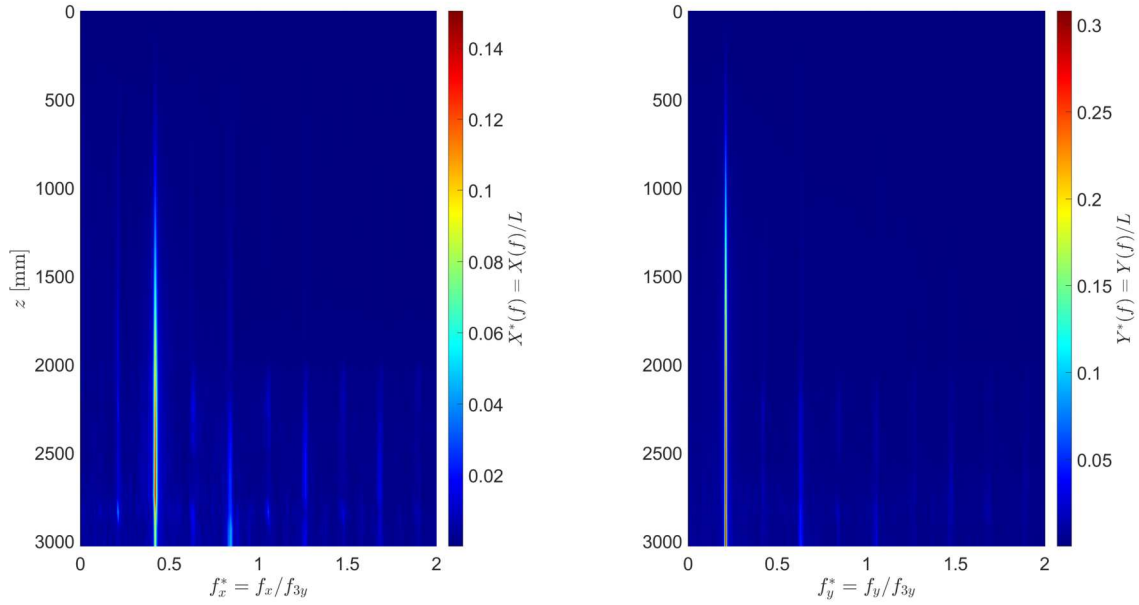

(a)

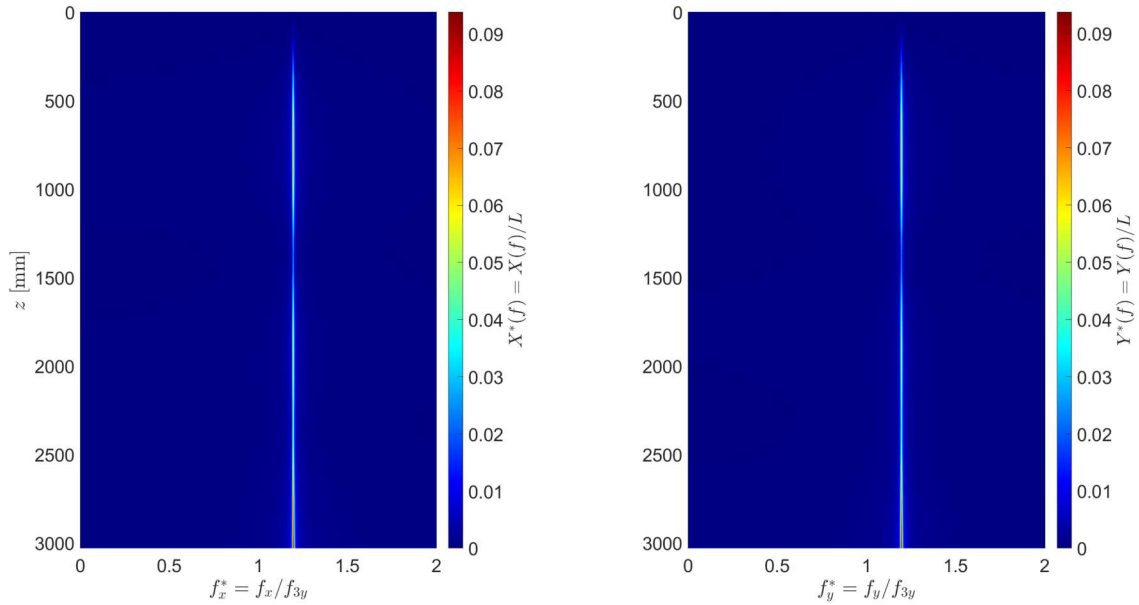

(b)

Figure 5. Amplitude spectra along the length of the model in the x and y directions. (a) Experimental model. (b) Numerical model.

5. CONCLUSIONS

Through an innovative experimental campaign, is was possible to assess the dynamics of a submerged cantilevered flexible pipe with a rigid ballast attached at its free end under dynamic excitation of discharging flow in the post-critical regime. In this paper, the mathematical model originally developed for aiding the design of the experiments and setting the parameters of the test scenarios was now confronted with the experimental results, in order to verify if the numerical simulation results were able to replicate the experimental ones. On one hand, the model was able to predict the approximate value of a critical discharging velocity, above which the vertical equilibrium configuration becomes unstable and a steady state non-linear oscillatory response with high amplitudes is observed, characterizing a Hopf bifurcation. The experimental model, however, exhibited even larger amplitudes in its three-dimensional motions, and an internal resonance with a 2:1 frequency ratio was identified in the responses.

In terms of the discrepancy in amplitude only, it should be noticed that the real part of the unstable eigenvalue is highly sensitive to small variations of the internal flow velocity slightly above the critical value. However, other hypotheses adopted for the numerical analysis such as considering the structure to be inextensible and modelling only the drag force for the fluid-structure interaction (given that the experiment was performed in steady water), might be more relevant for explaining significant differences in terms of motion pattern and frequency content in the experimental response. The evaluation of each of the aspects that are in disagreement between the numerical and the experimental results suggests that there are other aspects of fluid-structure interaction not accounted for in the numerical model, and that the axial dynamics plays a role in the developed movement that cannot be obtained with an inextensible model.

ACKNOWLEDGEMENTS

The authors deeply acknowledge Shell/2021 SWIR R&D Project FUSP 3456, the São Paulo State Research Foundation (FAPESP) for the support through the Thematic Project "Nonlinear Dynamics Applied to Engineering Systems", process 2022/00770-0, and Instituto de Pesquisas Tecnológicas do Estado de São Paulo (IPT) technical staff. W. A. Defensor-Filho acknowledges a PPGEN Capes scholarship. G. R. Franzini and C. Pesce acknowledge the National Council for Scientific and Technological Development (CNPq) research grants 305945/2020-3 and 307995/2022-4, respectively. G. R. Franzini also acknowledges FAPESP research grant 2022/02995-9.

REFERENCES

Benjamin, T.B., 1961. "Dynamics of a system of articulated pipes conveying fluid I. Theory." *Proceedings of the Royal Society of London, Series A*, Vol. 261, pp. 457–486.

Casetta, L. and Pesce, C.P., 2013. "The generalized Hamilton's principle for a non-material volume." *Acta Mech.*, Vol. 224, pp. 919–924.

Defensor Filho, W.A., Pesce, C.P., Vernizzi, G.J. and Maciel, V.S.F., 2023. "Experimental insights on the dynamics of submerged flexible pipes discharging water in post-critical regime." In *Proceedings of XIX the International Symposium on Dynamic Problems of Mechanics, DINAME 2023*. ABCM, Pirenópolis, Go, Brazil.

Orsino, R.M.M., Pesce, C.P. and Franzini, G.R., 2018. "A 3D non-linear reduced order model for a cantilevered pipe ejecting fluid under VIV." In *Proceedings of 9th International Symposium on Fluid-Structure Interactions, Flow-Sound Interactions, Flow-Induced Vibration Noise, FIV 2018*. Toronto, Canada.

Païdoussis, M.P., 1998. *Fluid-Structure Interactions: Slender Structures and Axial Flow, Vol. 1.* Academic Press, Oxford.

Païdoussis, M.P., 2022. "Pipes conveying fluid: A fertile dynamics problem." *Journal of Fluids and Structures*, Vol. 114, p. 103664.

Vernizzi, G.J., Maciel, V.S.F., Defensor Filho, W.A., Orsino, R.M.M., Franzini, G.R. and Pesce, C.P., 2023. "Dynamic small-scale riser model experiments: a physics-based algorithm to recover lost measurements from optical tracking systems." In *Proceedings of the ASME 2023, 42nd International Conference on Ocean, Offshore and Arctic Engineering, OMAE 2023*. Melbourne, Australia.